

## Diagnostic of Supercooled Clouds from Single-Doppler Observations in Regions of Radar-Detectable Snow

I. ZAWADZKI AND W. SZYRMER

*Cooperative Center for Research in Mesometeorology, and Department of Atmospheric and Oceanic Sciences, McGill University, Montreal, Quebec, Canada*

S. LAROCHE

*Cooperative Center for Research in Mesometeorology, and Atmospheric Environment Service of Canada, Montreal, Quebec, Canada*

(Manuscript received 6 November 1998, in final form 19 June 1999)

### ABSTRACT

Liquid water is produced in the updraft regions of subfreezing clouds when the generation of vapor excess over the water saturation value exceeds the vapor depletion through the depositional growth of the solid particles. A diagnostic technique for the presence of supercooled cloud in the presence of snow is presented here. The data required are single-Doppler observations of reflectivity and radial velocity as well as a nearby sounding of temperature. From these data, the 3D wind field is retrieved by a variational method. From the retrieved vertical motion, the supercooled water is derived from the steady-state balance relation between snow content and cloud liquid water. The method is tested with a kinematic model that includes the main microphysical processes expected to occur in stratiform subfreezing conditions. A comparison between aircraft in situ measurements of supercooled water content and the diagnosed as well as model-generated values shows good agreement.

### 1. Introduction

The accretion of supercooled droplets on an airframe affects the flight characteristics of an aircraft and causes serious hazards to flight operations (Cooper et al. 1984; Gayet et al. 1992; Rasmussen et al. 1992). Furthermore, the danger of icing becomes more important with the use of high efficiency airfoils more sensitive to surface contamination (Perkins 1995) and for operations at low altitude. Modica et al. (1994) state that the U.S. Air Force, for example, has turned to low-level flight as a means of increasing the survivability of its aircraft during certain tactical operations.

Supercooled cloud liquid water (SCW) is also considered as a very significant indicator of precipitation potential having relevance for weather modification (Sassen et al. 1990). Moreover, SCW plays an important role in the wet removal of chemical species from the atmosphere: cloud droplets serve as tiny pollutant reservoirs within the cloud and, in the riming process, pollutants are transferred to the cleaner snow crystals

grown by vapor diffusion (Devulapalli and Collett 1994; Dixon et al. 1995). SCW that is collected by falling ice particles affects the precipitation parameters (e.g., particle number concentration; Waldvogel et al. 1993) and may also influence the form of precipitation on the ground since the vertical extent of the melting layer is determined by the size and density of melting crystals that strongly depend upon the degree of crystal riming. Freezing of supercooled droplets may also lead to ice multiplication (Hallett and Mossop 1974). Ultimately, the SCW influences the radiation balance of the atmosphere (e.g., Sassen et al. 1985). Thus, the prediction and detection of the SCW remains a focus of cloud physicists.

In a study of the development of microphysics in an Atlantic storm, Zawadzki et al. (1993a, henceforth to be referred to as ZOL) showed that during the development of a precipitating system, the SCW appears as a transient phenomenon during the uplift of initially clear air. Once precipitation develops within the supercooled cloud and snow grows at the expense of the liquid, SCW vanishes rapidly. It is also possible for SCW to coexist at equilibrium with snow if the vertical air motion is strong enough so that the rate of the generation of water vapor excess overcomes the rate at which snow grows by deposition.

---

*Corresponding author address:* Isztar Zawadzki, Department of Atmospheric and Oceanic Sciences, McGill University, 805 Sherbrooke St. W., Montreal, PQ H3A 2K6, Canada.  
E-mail: isztar@zephyr.meteo.mcgill.ca

In this work we develop a diagnostic method for SCW in regions where the radar detects precipitation. The method is intended to apply to stratiform snow precipitation in situations where equilibrium between the microphysical processes and vertical air motion can be assumed. The retrieval algorithm comprises the following steps: first, evaluation of the snow content from radar data at the temperature and pressure conditions given by a nearby sounding. Second, retrieval of the 3D winds from single-Doppler measurements using the method described by Laroche and Zawadzki (1994) and Kilambi et al. (1995). Finally, calculation of the equilibrium liquid water content, that is, the liquid water that can be sustained at steady state in the presence of the measured amount of snow under the retrieved updraft.

The validation of the method is done through numerical experiments using a 3D kinematic microphysical model. The model is initialized by the retrieved winds (whereas the snow content derived from the radar measurements is not used as input); when steady state is reached the fields of the various hydrometeors are analyzed. If the model reproduces the radar observed snow well, then equilibrium conditions are confirmed, and the amount of SCW can be diagnosed from the model output and compared to the equilibrium SCW. The method is further tested by comparing the diagnosed amount of SCW with one in situ aircraft observation.

Other techniques that determine the amount of SCW by assuming a steady-state distribution have been developed previously. For instance, the steady-state balance relation for the coexistence of SCW and snow was used by Murakami et al. (1992) to analyze the microphysical structure and precipitation mechanism associated with warm frontal clouds. Tremblay et al. (1995) used a similar approach to generate icing forecasts based on the mesoscale model outputs. Section 2 presents a theoretical study of the conditions necessary for the steady-state existence of supercooled clouds in the presence of precipitation. Section 3 discusses the SCW diagnosis directly from reflectivity data. Section 4 presents the wind retrieval technique from single-Doppler radar data used to diagnose the amount of SCW. The next section describes the kinematic model used to validate the proposed method. The first simulation of an episode of winter storm, presented in section 6, verifies the self-consistency of the method. The second, described in section 7, reproduces the conditions of aircraft liquid water measurements obtained within the stratiform precipitation associated with a warm front. Concluding remarks are drawn in section 8. All symbols used in the paper are defined in appendix C. All mathematical expressions are expressed in SI units.

## 2. Coexistence of SCW and snow

Let us first identify the conditions necessary to produce and maintain SCW in the presence of precipitating

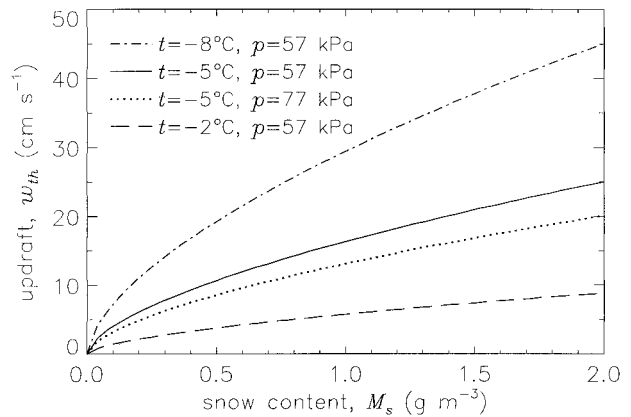


FIG. 1. Threshold value of vertical velocity that can generate SCW as a function of snow content for selected temperatures and pressures.

snow. The main microphysical processes that could be active in this situation are presented in appendix A (Fig. A1). However, only some of them are included in our analysis following a number of simplifying conditions that will be adopted here.

- 1) In the presence of supercooled clouds, the air is saturated with respect to water.
- 2) Precipitating snow and ice clouds are in separate regions of the cloud system (ice above and snow below, as shown by ZOL) and ice multiplication processes are not included. In the situations studied here, the specific conditions for the Hallett–Mossop mechanism, the predominant ice enhancement, are not fulfilled in general.
- 3) The SCW content coexisting in equilibrium with snow is low enough (below  $0.5 \text{ g m}^{-3}$ , see ZOL) so that there is no conversion of snow into graupel.
- 4) The system is at steady state.

With the second and third assumptions snow can be considered the only water condensate interacting with SCW. In these conditions, the rate of change of supersaturation  $s_w$ , within a parcel of cloudy air ascending with velocity  $w$ , can be written in a form similar to that derived for liquid cloud [cf. Pruppacher and Klett 1997, Eq. (13.30)]:

$$\frac{ds_w}{dt} = \alpha_1 w - \alpha_2 \text{DEPvs} - \alpha_3 \text{CNDvc}, \quad (1)$$

where  $\alpha_1$ ,  $\alpha_2$ , and  $\alpha_3$  are thermodynamic parameters given by

$$\alpha_1 = \frac{\varepsilon L_v g}{R' c_p T^2} - \frac{g}{R'T}, \quad \alpha_2 = \frac{R'T}{\varepsilon e_s(T)} + \frac{\varepsilon L_v L_s}{p T c_p},$$

$$\alpha_3 = \frac{R'T}{\varepsilon e_s(T)} + \frac{\varepsilon L_v^2}{p T c_p}.$$

The terms CNDvc and DEPvs describe the rate of water vapor depletion ( $\text{kg m}^{-3} \text{ s}^{-1}$ ) through condensation on

supercooled cloud droplets and deposition onto snow particles, respectively. Appendix C contains variable definitions.

The steady-state assumption in a Lagrangian framework ( $ds_w/dt = 0$ ), with the approximation:  $\alpha_2 \approx \alpha_3$ , leads to the following balance relationship:

$$wG - \text{DEPvs} - \text{CNDvc} = 0, \quad (2)$$

where  $wG$  represents the rate at which the excess of water vapor above the saturation value is produced,  $G = -\rho \partial r_s / \partial z$  is the generating function,  $r_s$  is the saturation mixing ratio with respect to water. Using the Clausius–Clapeyron equation,  $G$  can be expressed as

$$G = \left[ (\Gamma_w - \Gamma_d) \frac{c_p}{L_v} - \frac{gr_s}{R'T} \right] \rho.$$

From the above relation  $G$  can be calculated if temperature and pressure are known.

#### a. Threshold conditions for SCW production

Equation (2) shows that CNDvc, the source of SCW, results from the imbalance between the terms  $wG$  and DEPvs. This implies that the liquid water production is possible only if the snow amount is insufficient to bring the available moisture below the saturation with respect to water. Thus, the vertical motion required for the occurrence of supercooled cloud water can be determined from

$$wG \geq \text{DEPvs}, \quad (3)$$

where DEPvs is obtained by assuming water saturation. The same criterion for formation of SCW was proposed by Heymsfield (1977), ZOL, and Tremblay et al. (1995). Also Rauber and Tokay (1991) used an equivalent relation to explain the existence of supercooled water at the top of cold clouds in the presence of ice crystals.

The values of threshold vertical velocity obtained from (3):

$$w_{\text{th}} = \frac{\text{DEPvs}|_{M_c=0}}{G}, \quad (4)$$

are shown in Fig. 1. The term DEPvs is calculated using (A14):

$$\text{DEPvs}|_{M_c=0} = \alpha(C_1 M_s^{0.5} + C_2 \vartheta M_s^{0.66}), \quad (5)$$

where the two fall speed constants and the snow density, specified in appendix A, are introduced. This relation describes the depositional growth of snow in water saturated atmosphere in the absence of SCW. The terms  $\alpha = 2\pi\phi_i[(e_s/e_{si}) - 1]$  with  $\phi_i$  defined by (A7) and  $\vartheta$  defined by (A8), are thermodynamic functions, while  $C_1$  and  $C_2$  are expressed in terms of microphysical parameters as follows:

$$C_1 = 0.049N_{os}^{0.5} \quad \text{and} \quad C_2 = 0.021N_{os}^{0.34}$$

with  $N_{os}$  in  $\text{m}^{-4}$ .

The atmospheric conditions of 57 kPa and  $-5^\circ\text{C}$ , used in the calculation of  $w_{\text{th}}$  in Fig. 1, correspond to the conditions prevailing during the aircraft in situ measurements presented in section 7.

#### b. Steady-state SCW coexisting with snow precipitation

For equilibrium between the various microphysical processes to be possible, the time constant of each process must be short compared to the rate of change of the vertical motions. The processes relevant here are condensation, deposition, and the process of snow riming, SCCcs. Condensation and deposition are very fast processes. Thus, in weak to moderate updrafts, equilibrium between water vapor and condensate can be safely assumed. The same is not obvious for the riming process. Consequently, we should evaluate the time constant  $\tau$  of the depletion of liquid cloud water by snow from

$$\frac{dM_c}{dt} = -\text{SCCcs}. \quad (6)$$

We use the parametric expression for SCCcs derived from (A13) given in appendix A:

$$\text{SCCcs} = \beta M_c M_s^{0.82}, \quad (7)$$

$M_c$  (the SCW content) and  $M_s$  are in  $\text{kg m}^{-3}$  and SCCcs is in  $\text{kg m}^{-3} \text{ s}^{-1}$ , and  $\beta = 0.079N_{os}^{0.18}(\rho_0/\rho)^{0.5}$  (with  $N_{os}$  given in  $\text{m}^{-4}$ ) is a weak function of temperature, pressure, and microphysical parameters.

$$M_c = M_{c0} e^{-(t/\tau)},$$

For  $M_s$  constant in time, the solution for  $M_c$  is where  $M_{c0}$  is  $M_c$  at the initial time. The time constant,  $\tau$ , is given by  $\tau = (\beta M_s^{0.82})^{-1}$  and is independent of  $M_c$ . However, this result overestimates the value of the time constant since  $M_s$  increases continually during the time interval  $[0, \tau]$  due to the mass transferred to snow by riming. A better estimation of  $\tau$  can be obtained by replacing the value of  $M_s$  for  $t = 0$  by its average value between  $t = 0$  and  $t = \tau$  giving

$$\tau \approx (\beta M_s^{0.82})^{-1} \left( 1 + \frac{e M_{co}}{2 M_s} \right)^{-0.82}. \quad (8)$$

This expression can be used as the approximate solution of (6) with  $M_s$  increasing over time. In compressible atmosphere, the term accounting for air expansion that accompanies updraft,  $-kwM_c$  [as in the conservation equation for snow (14)], is omitted in (6). This leads to a slight overestimation of the time constant defined by (8). The overestimation is more important in stronger updrafts and lighter snowfall.

The curves in Fig. 2 show the dependence of  $\tau$ , obtained from (8), as a function of  $M_s$  for two values of air density and two assumed ratios  $M_{co}/M_s$ . As shown

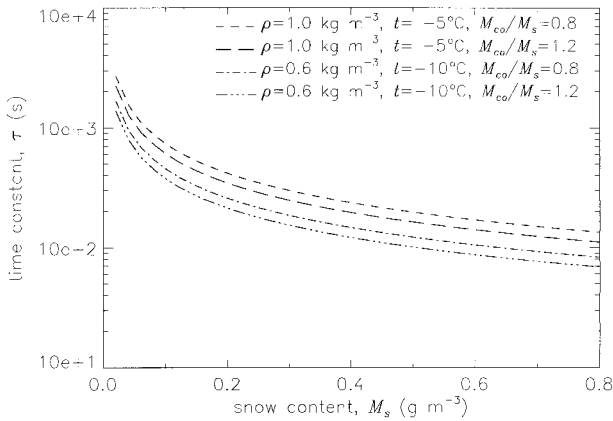


FIG. 2. Approximate value of time constant for cloud liquid water content to be depleted by riming of snow as a function of snow content. Two values of air density ( $1.0 \text{ kg m}^{-3}$  and  $0.6 \text{ kg m}^{-3}$ ) and temperature ( $-5^\circ$  and  $-10^\circ\text{C}$ ) are used for this calculation. The assumed ratios of initial liquid water content to snow content are 0.8 and 1.2.

in Fig. 2, for a typical snow content ( $M_s = 0.2 \text{ g m}^{-3}$ ),  $\tau$  is approximately 5 min.

From the above discussion it can be deduced that for conditions where snow is present for several minutes, the equilibrium between SCW and snow can also be assumed. The assumption of equilibrium imposes the balance of SCW depletion and SCW production. That is, under the simplifying conditions described here, the rate of removal of SCW by snow riming equals to the rate of condensation within an updraft:

$$\text{CNDvc} \approx \text{SCCcs}. \quad (9)$$

Combining (2) and (9) gives the relation describing the steady-state relationship between updraft, snow content, and cloud liquid water content:

$$wG \approx \text{DEPvs} + \text{SCCcs}. \quad (10)$$

Because the sum of deposition and riming rates gives the source term for snow growth  $S_s$ , (10) can be also written as

$$wG \approx S_s. \quad (11)$$

Thus, in other words, the steady-state relationship expresses the fact that the rate at which water vapor becomes available for condensation/deposition equals the rate of water transferred to precipitation via deposition and riming, as was shown by Zawadzki et al. (1993b) in stratiform precipitation.

The parametric expression for DEPvs in terms of snow content is obtained from (A14) in appendix A:

$$\text{DEPvs} = \text{DEPvs}|_{M_c=0} - \chi \text{SCCcs}, \quad (12)$$

where  $\text{DEPvs}|_{M_c=0}$  is given by (5) at water saturation and  $\chi(T, p)$  defined in (A9). Since air containing cloud liquid water is considered to be close to water saturation, regardless of the magnitude of SCW content, DEPvs mainly depends on the precipitation content, air tem-

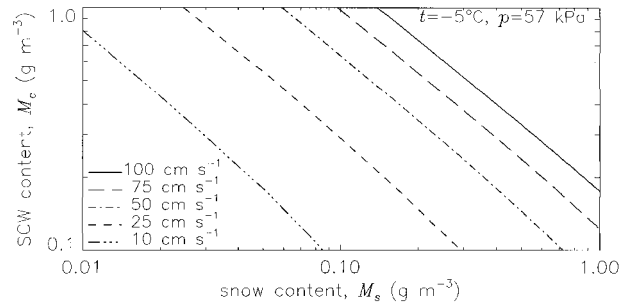


FIG. 3. Cloud liquid water content as a function of the snow content as predicted by (13) for four updraft velocities. A temperature of  $-5^\circ\text{C}$  and a pressure of 57 kPa are used for this calculation.

perature, and pressure. On the other hand, the rate at which cloud water is collected by precipitating snow, SCCcs, given by (7), is proportional to the amount of SCW. Thus, for a given temperature, pressure, and precipitation amount, the vertical motion determines the quantity of liquid water that must be available for collection so that the equilibrium condition described by (10) can be established.

Therefore, (10) gives an estimation of the steady-state SCW content that can coexist with snow. After introducing into (10) the parametric expressions for SCCcs and DEPvs, given by (7) and (12), respectively, we can explicitly solve for  $M_c$ :

$$M_c = \frac{1}{\beta(1 - \chi)M_s^{0.82}}(wG - \text{DEPvs}|_{M_c=0}).$$

Substituting (4) into (12), this relation can also be written as

$$M_c = \frac{G}{\beta(1 - \chi)M_s^{0.82}}(w - w_{\text{th}}).$$

Introducing the parametric description of  $\text{DEPvs}|_{M_c=0}$ , given by (5), yields

$$M_c = \frac{1}{\beta(1 - \chi)M_s^{0.82}}[wG - \alpha(C_1 M_s^{0.5} + C_2 \vartheta M_s^{0.66})]. \quad (13)$$

This relation will be used to retrieve the steady-state SCW distribution.

The last relations show the linear dependence of  $M_c$  with respect to the updraft magnitude for given atmospheric and snow conditions. This dependence is more important in light precipitation since the slope is proportional to  $M_s^{-0.82}$ . It expresses the fact that the riming rate on smaller snow content has to increase more rapidly with the intensified production of SCW in order to assure equilibrium conditions. Since  $\text{DEPvs}|_{M_c=0}$  (and  $w_{\text{th}}$ ) is a very weak function of  $M_s$ , for specific values of  $w$ ,  $T$ , and  $p$ , the amount of SCW is expected to be nearly inversely proportional to the snow content. Figure 3 shows the value of  $M_c$ , predicted by (13), as a function of snow content for four different updrafts. The

inverse correlation between liquid water measurements and the intensity of snow precipitation was also reported, among others, by Heggli et al. (1983) and Rauber et al. (1986). The steady-state SCW depends also on temperature, and to lesser extent, on pressure, both necessary to estimate the functions  $G$ ,  $\beta$ , and  $\chi$ , and the thermodynamic functions used to describe  $\text{DEPvs}|_{M_c=0}$ . The increase of  $M_c$  with temperature is rather weak for all except light snow precipitation and strong updrafts.

It can be noted that  $M_c$  is also sensitive to the assumed microphysical parameters. Given the natural variability of snowflake parameters in real atmospheric conditions, the amount of SCW deduced from (13) has to be considered as an approximate estimation of the SCW distribution. A discussion on the uncertainties in the inferred SCW due to uncertainties of the input parameters is presented in appendix B.

The thermodynamic conditions required to calculate the SCW content from (13) can be obtained from a nearby sounding, while the snow content can be estimated from radar data. The main difficulty in the use of (13) for SCW diagnosis is in the estimation of  $w$ . The next two sections are devoted to this problem.

Some simplifications can be introduced to (13): (a) since the ratio  $C_1 M_s^{0.5} / C_2 v M_s^{0.66}$  is greater than 100 for any temperature lower than  $-2.5^\circ\text{C}$  and for snow content greater than  $0.05 \text{ g m}^{-3}$ , the term  $C_2 \partial M_s^{0.66}$  can be neglected; (b)  $\chi$  can be also omitted because its value remains lower than 0.08 in the range of atmospheric thermodynamic conditions. These simplifications lead to the approximate form of (13) given by

$$M_c \approx \frac{1}{\beta M_s^{0.82}} (wG - \alpha C_1 M_s^{0.5}), \quad (13')$$

where

$$\beta = \frac{\Gamma(3+b)}{4\rho_s} (\pi\rho_s N_{os})^{0.25(1-b)} aE_{sc} \left( \frac{\rho_w}{\rho} \right)^{0.5} \quad \text{and}$$

$$C_1 = 0.86 \left( \frac{\pi\rho_s}{N_{os}} \right)^{0.5}$$

with  $\alpha$  denoting a thermodynamic function at water-saturated conditions as introduced in (5).

### 3. Assessment of SCW with $w$ estimated from reflectivity

The conservation equation for snow, describing the distribution of precipitation as developed by Kessler (1969), can be written as

$$\frac{dM_s}{dt} + w \left( \frac{\partial M_s}{\partial z} + kM_s \right) + \frac{\partial(M_s \bar{V}_s)}{\partial z} = S_s, \quad (14)$$

where  $\bar{V}_s$  is the snow fall speed and  $k$  is the air compressibility term (i.e.,  $k = -\partial \ln\rho / \partial z \approx 10^{-4} \text{ m}^{-1}$ ). Sub-

stituting (11) into (14) leads to the following expression for  $w$ :

$$w = \frac{\frac{dM_s}{dt} + \frac{\partial(M_s \bar{V}_s)}{\partial z}}{G - \left( \frac{\partial M_s}{\partial z} + kM_s \right)}. \quad (14')$$

In principle, the right-hand side can be evaluated from radar measurements and a nearby sounding (Zawadzki et al. 1993b). Heymsfield (1977) derived a similar expression for  $w$ , the so-called mass-flux technique, which is based on the assumption that there is no net accumulation of water substance in any fixed layer in a steady-state cloud.

Introducing (14') in (13) gives the relation allowing SCW content to be estimated from the snow field, its vertical gradients, and thermodynamic air conditions:

$$M_c = \frac{1}{\beta(1-\chi)M_s^{0.82}} \left[ \frac{\frac{dM_s}{dt} + \frac{\partial(M_s \bar{V}_s)}{\partial z}}{1 - \frac{1}{G} \left( \frac{\partial M_s}{\partial z} + kM_s \right)} - \text{DEPvs}|_{M_c=0} \right]. \quad (15)$$

However, there are some difficulties related to the use of vertical motion retrieved in this manner for the diagnosis of SCW. To illustrate this, let us introduce in (15) additional simplifications: take  $\bar{V}_s$  as a constant at  $1 \text{ m s}^{-1}$ , neglect the compressibility term, assume  $G \gg \partial M_s / \partial z$  (quite true in stratiform precipitation) and assume that the system is in a steady state in a moving reference frame. All these simplifications lead to the approximate expression for  $wG$ :

$$wG \approx \bar{V}_s \frac{\partial M_s}{\partial z}. \quad (16)$$

Suppose that  $\text{DEPvs}$  and  $\text{SCCs}$  are linearly dependent with respect to  $M_s$ . Then (12) and (7) simplify to

$$\text{DEPvs} = \alpha' M_s \quad \text{and} \quad \text{SCCs} = \beta M_c M_s, \quad (17)$$

where  $\alpha'$  and  $\beta$  depend on thermodynamic and microphysical parameters. Using all the above approximations, the expression for SCW, deduced from (10), reduces to:

$$M_c = \frac{\bar{V}_s}{\beta} \frac{\partial \ln M_s}{\partial z} - \frac{\alpha'}{\beta}.$$

This equation shows that the amount of cloud water that coexists at equilibrium with snow is basically given by the vertical gradient of snow content and thermodynamic conditions.

It is clear that the main difficulty of using (15) to retrieve SCW content lies in the conversion from radar equivalent reflectivity to the gradient of  $M_s$ . Most cases where the SCW content could be important will occur

in relatively warm regions of a snow storm, between 0°C and -6°C, where probably most of the snowflake aggregation takes place. The vertical gradient of reflectivity will reflect this aggregation as well as snow growth by riming and deposition. To separate the effects of aggregation from the effects of growth on the reflectivity gradient is a difficult task.

The problem of estimating the vertical gradient of snow content can be avoided if  $M_c$  is estimated using (13) without using (14') to evaluate  $w$ . In the next section, we explore an alternative method for the retrieval of the vertical velocity  $w$ .

#### 4. Retrieval algorithm for SCW content from single-Doppler radar data

The alternative method for diagnosing SCW relies on relation (13) and the vertical motion obtained by a variational method for the retrieval of the 3D wind field from single-Doppler radar observations described by Laroche and Zawadzki (1994). In this technique, Doppler radial velocities and the continuity equation are used together with the conservation of snow to retrieve  $w$ . Therefore, the uncertainty in the conversion from reflectivity to snow content, noted in the previous section, is less critical.

Since the calculation of the wind field is an important part of the SCW estimation, a brief description of the variational analysis used for the 3D wind retrieval is first presented.

The constraining model used for the retrieval of the 3D wind field is formed by the anelastic continuity

$$\frac{\partial u}{\partial x} + \frac{\partial v}{\partial y} + \frac{\partial w}{\partial z} = kw, \quad (18)$$

and the conservation equation for snow (14) in which  $M_s$  and  $V_s$  are estimated from the reflectivity  $Z$  by using the following relationship (Zawadzki et al. 1993b):

$$M_s = 10^{-5} Z^{0.5}, \quad (19)$$

$$\bar{V}_s = -0.82Z^{0.063} \left( \frac{\rho_o}{\rho} \right)^{1/2}. \quad (20)$$

The source or sink term  $S_s$  is assumed to be equal to  $wG$  as in (11). The anelastic continuity equation is used as a strong constraint while the equation for the conservation of precipitation is used as a weak constraint.

The horizontal wind field is defined as

$$u(x, y, z) = U + u'(x, y, z), \quad (21a)$$

$$v(x, y, z) = V + v'(x, y, z), \quad (21b)$$

where  $u'$  and  $v'$  are the wind components in a reference frame moving at  $(U, V)$ . The wind field is retrieved in two steps:

- 1) The velocity of the moving frame is retrieved by minimizing the following cost function:

$$J(U, V) = k_v \sum_{n=1}^{N-1} \epsilon_{vn}^T \epsilon_{vn} + k_M \sum_{n=1}^{N-1} \epsilon_{Mn}^T \epsilon_{Mn}, \quad (22)$$

where the wind components  $(u', v', w)$  are set to zero,  $N$  is the number of volume scans used for the retrieval,  $\epsilon_{vn}$  is a vector containing the differences between the observed radial velocities and the corresponding values of the steady-state wind field at time  $n$ ,  $\epsilon_{Mn}$  are the residuals of the conservation equation,  $k_v$  and  $k_M$  are constant weights, and  $T$  stands for the transpose. For the results presented in this paper,  $k_v$  and  $k_M$  were set to 1.0 as in Kilambi et al. (1995).

- 2) The wind components  $u'$ ,  $v'$ , and  $w$  are then retrieved by minimizing the following cost function:

$$J(u', v', w) = k_v \sum_{n=1}^{N-1} \epsilon_{vn}^T \epsilon_{vn} + k_M \sum_{n=1}^{N-1} \epsilon_{Mn}^T \epsilon_{Mn} + J_2(u') + J_2(v'), \quad (23)$$

where  $J_2$  is a smoothness constraint as defined by Wahba and Wendelberger (1980). The minimization procedure as well as how the weights are prescribed and presented in Laroche and Zawadzki (1994).

We will use the wind velocity in the regions of radar detectable snow, retrieved by the technique described above, to diagnose the SCW amount from (13). The single-Doppler observations and the nearby sounding (for temperature and pressure information) are the only data required by this technique.

#### 5. Description of the kinematic microphysical model

The method described in the previous section makes use of a number of simplifying assumptions about microphysical processes. Here, we validate the procedure using a kinematic microphysical model in which most of these assumptions are not included.

The retrieved wind field is used to drive a bulk microphysics parameterization package from which the fields of snow and liquid water contents are obtained. The agreement between the model-derived field of  $M_s$ , and radar-observed values would strengthen confidence in the model-derived values of SCW content. We develop the methodology using observations from the case of the heavy snow precipitation system on 13–14 March 1993 in the Montreal area, in which no SCW was expected within the simulated domain, and then apply the model to the conditions of stratiform precipitation associated with a warm front on 21 October 1993 in the area where a research aircraft gathered in situ liquid water measurements.

##### a. Microphysics parameterization

The microphysics parameterization used here is an extension of the one described in ZOL. It is a bulk-type

parameterization in which all the water content is divided between water vapor, liquid cloud, ice cloud, rain, snow, and graupel/hail. The temperature and mixing ratios of each of the water species are carried as prognostic variables in the model. It is assumed that each of the condensate is distributed according to a specified continuous particle size distribution. The information about distributions in the model is given in appendix A.

The thermodynamic equation for temperature and mass continuity equations for mixing ratios follow the approach proposed by Kessler (1969). The terminal velocity for the various water species is a mass-weighted average. For a small amount of precipitation a lower limit on the terminal fall velocity of snow is imposed as suggested by Burrows (1992).

Hydrometeors and water vapor can interact in the model via 41 microphysical processes. Each of them represents the rate at which one water species is transformed into another per unit volume of air. The expressions for microphysical processes and terminal velocities of each hydrometeor category are given in terms of moments of the particle size distribution, allowing flexibility in the assumed form of distributions. A list of all the processes that were activated in the described experiments, their schematic representation, along with the nomenclature employed, can be found in appendix A. In addition, the development of the parametric expressions of the two principal processes involved in the SCW retrieval algorithm (snow growth by deposition and riming) is presented.

The following briefly explains the rank in which the different processes appear in the model calculations as well as the main departures from the description given in ZOL. The processes with the highest priority are the ones responsible for the initiation of cloud particles (primary nucleation of ice by deposition and activation of cloud condensation nuclei). The second priority is given to the processes describing the growth of cloud and precipitation particles by diffusion of vapor. The main differences from the treatment of processes of vapor transfer described in ZOL are the following.

- 1) The activation of cloud condensation nuclei is prescribed so that all the vapor excess with respect to liquid water is condensed immediately (we assume that a sufficient number of nuclei is always available) and the grid box volume is returned to saturation at the warmer temperature resulting from the released latent heat of condensation. The nucleation of the liquid phase is performed only in the absence of cloud droplets.
- 2) The nucleation of ice by deposition/condensation freezing is modeled as proposed by Ferrier (1994), that is, at temperatures warmer than  $-5^{\circ}\text{C}$ , the process is described by the relation given by Cotton et al. (1986) and Murakami (1990), while at colder temperatures the rate of nucleation follows the formulation proposed by Meyers et al. (1992).
- 3) The diffusional growth of existing drops (cloud or rain) is determined by requiring that the exchange of sensible heat between the droplets and the air be balanced by the latent heat associated with the phase change. Consequently, some supersaturation with respect to water is allowed to coexist within liquid clouds.
- 4) In the presence of SCW, the calculation of the depositional growth of solid hydrometeors takes into account their temperature increase resulting from the release of latent heat during freezing of the collected droplets.
- 5) If necessary, the mass transfer between vapor and the various categories of hydrometeors is performed only after the adjustment of all diffusional growth processes activated at a given grid point. These processes are determined depending on the state of vapor saturation after the vapor exchange via the initiation processes; the adjustment must be done if too much drying or moistening of the environment takes place due to the summation of vapor transfers calculated independently for each activated process.

The formation of cloud ice by homogeneous and heterogeneous freezing of cloud water follows the diffusion processes. The homogeneous nucleation of ice from liquid droplets is assumed to take place instantaneously whenever temperature is below  $-35^{\circ}\text{C}$ , while the rate of the heterogeneous freezing depends on the degree of supercooling and the droplet size. The parameterization of the last process is taken from Murakami (1990). It follows the growth of snow by collection processes and, then, the autoconversion of cloud ice particles forms precipitating snow as described in ZOL.

#### *b. Kinematic numerical model*

The parameterization of the microphysical processes was coupled with the wind fields retrieved from Doppler radar data to form our 3D kinematic numerical model. At steady state, it reproduces the spatial distribution of temperature and hydrometeors contents at equilibrium with the prescribed wind field.

The wind retrieval technique can be applied only where radar observations are available. In stratiform precipitation, cloud extends well above the radar returns, indicating vertical motions above the radar detectable precipitation. Therefore, a simple upward linear interpolation of the wind components, assuming zero values in the upper layer of the model, is performed in regions free of data. Zawadzki et al. (1993b) showed that winds at high altitudes do not have a significant influence on the steady-state solution for the microphysical fields in the lower levels. The lack of humidity at very low temperatures prevents the formation of precipitation, and the fall speed of ice crystals is too weak to couple the microphysics at the upper levels with the lower levels.

Thus, the extrapolation required by the model is not critical for our objectives.

The model is initiated with horizontally uniform temperature and humidity fields. The air density profile is determined from the temperature versus pressure sounding and remains constant with time and space. Thus, changes in pressure are allowed wherever changes in temperature occur. The cloud hydrometeor fields (ice or liquid water) start at zero within the domain.

Top boundary conditions are rigid, with all variables held constant. In the two simulated events, the bottom of the model is set at the lowest level of the wind retrieval domain (1.5 and 4 km above the ground in the first and second simulations, respectively) and the vertical motion does not vanish at this first level. At the lateral inflow boundary, as well as at the lower boundary, the temperature and water vapor mixing ratio are maintained at the initial values. The precipitation is allowed to fall through the bottom of the domain.

At the lateral boundary the nonobserved fields of mixing ratios of the liquid cloud and ice cloud are either set to zero (in the second simulation) or change to allow horizontal continuity in the fields (in the first simulation). In the latter case, when advecting material from outside of the domain, the values at the boundary prior to advection are attributed to the advected material. This type of boundary condition is referred to as persistence.

The prognostic equations are integrated in time with a three time level semi-Lagrangian scheme. The time step is set to 5 s for all simulations presented here. The horizontal resolution is 4 km in the first case study and 1.5 km in the second. The vertical grid spacing is constant and set to 250 and 125 m in the first and second simulated cases, respectively. Since the corresponding radar data resolutions are 500 and 250 m, linear interpolation is used to introduce the wind field at intermediate levels in the model. There is no explicit treatment of diffusion in the model. The results shown below correspond to the steady state of model outputs.

## 6. Case study of 13–14 March 1993

### a. Overview of the case

On 12 March a very intense storm began to develop in the Gulf of Mexico. The cyclone was termed the “storm of the century,” for its hurricane force winds, total precipitation, and low pressure records. For a complete synoptic overview of the storm, see Huo et al. (1995). From 12 to 14 March, the storm moved northeastward, and at 0400 EST 14 March, its low center passed south of Montreal. The episode chosen for simulation occurred during the most intense period of the storm during its passage over Montreal (from 2300 UTC 13 March to 0300 UTC 14 March). The winds were blowing from the northeast near the surface at about  $10 \text{ m s}^{-1}$  and veering clockwise from the south-southwest at higher levels, giving nearly a  $180^\circ$  directional shear.

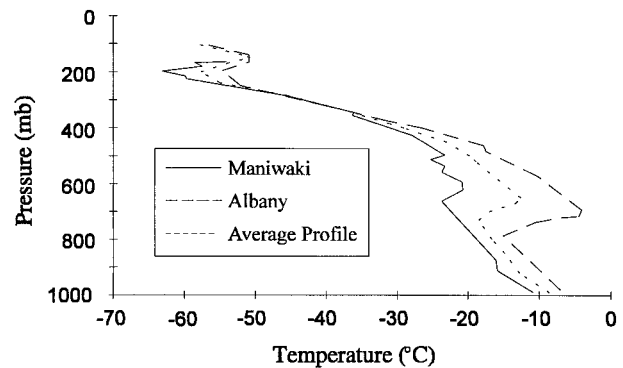


FIG. 4. Temperature profiles of Albany and Maniwaki for 0000 UTC 14 Mar 1993. The average profile should be representative of the Montreal region.

The wind speeds observed near the top of the storm were up to  $60 \text{ m s}^{-1}$ . Figure 4 shows the temperature profile of Albany and Maniwaki at 0000 UTC 14 March. During the episode, the temperature was below  $0^\circ\text{C}$  everywhere in the vertical excluding the presence of a melting layer over the region of interest.

### b. Retrieved 3D wind field

The wind field is retrieved from Doppler radar data from 0001 to 0011 UTC 14 March 1993 in an area of  $78 \text{ km} \times 78 \text{ km}$  east of the J.S. Marshall Radar Observatory (MRO) Doppler radar. (Appendix D summarizes the main characteristics of the radar.) Figure 5 shows the results of the retrieval at three different altitudes. As can be seen on the left-hand side of the figure, little horizontal variation in horizontal winds is observed. However, strong veering with height is very well defined. The vertical velocities field, given by the solid contours on the right-hand side of Fig. 5, contains detailed small-scale variability consistent with height. Vertical motion to  $30 \text{ cm s}^{-1}$  is obtained. The shadings in the figure represent the reflectivity field transformed into equivalent water content. No retrieval was performed on missing data points, located in the blank regions in Fig. 5.

The retrieved wind field is verified by comparison with the data from a 915-MHz wind profiler operating in downtown Montreal. For more details about the profiler, see Rogers et al. (1994). Figure 6 shows the profile of the horizontal components of the wind as calculated by the variational method at 1906 EST 13 March, along with the ones measured by the profiler at different times around the retrieval time. The values for the retrieval were taken from the column in the grid space that is the closest to the profiler. The profiler curves were obtained from 30-min consensus averages of the measurements. In general, the retrieved wind fields agree well with the profiler observations. However, at around 4.5 km the retrieval underestimated the strength of the wind due to beam-filling problems.

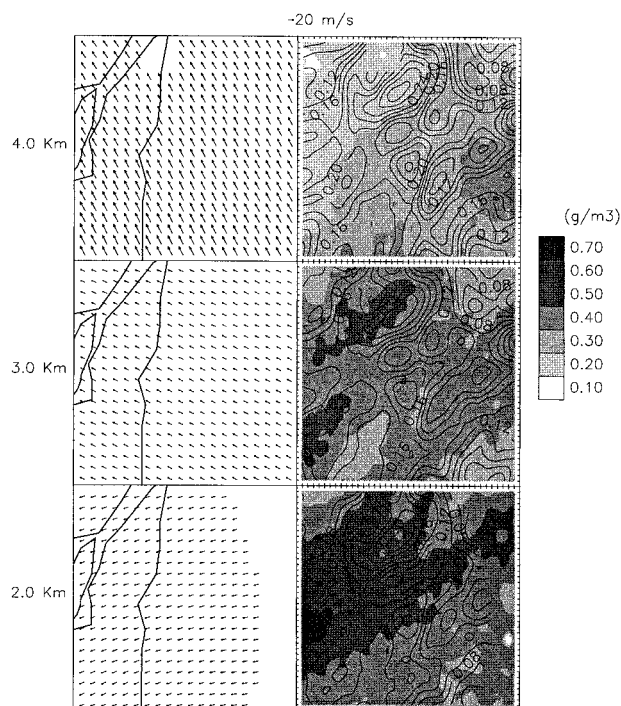


FIG. 5. Three-dimensional wind field retrieval at 0006 UTC 14 Mar 1993. The domain size is 78 km  $\times$  78 km. The left-hand side of the figure represents the horizontal wind, and the contours on the right-hand side give the vertical motion at 0.02 m s<sup>-1</sup> intervals. Shadings represent snow content (g m<sup>-3</sup>) corresponding to the observed reflectivity field. The jagged lines on the vector plots represent the terrain features.

*c. Setup of numerical simulations*

The simulations are performed on a horizontal domain of 76 km  $\times$  44 km that is a subdomain of the wind retrieval region located in an area where the absence of ground echoes provides good wind field retrieval and a good potential for comparison of the observed precipitation of snow and the one resulting from the model output. The model simulations are run with the winds calculated for 0006 UTC, when the storm's maximum intensity was within radar coverage. Temperature is initiated following the average profile of Fig. 4. The model bottom is set at 1.5 km and the top at 9.5 km. The results of the tests conducted to choose the horizontal resolution showed only minor differences when using a 2-km resolution of radar data or a coarser 4-km resolution. Therefore, the latter one is employed in the simulations described here.

At the lateral boundaries the snow derived from reflectivity data is used. For the nonobserved hydrometeor fields, persistence is used. Thus, it is necessary to assess how the retrieval of SCW content by the model can be affected by the forcing at the inflow boundary. Since the average wind speed in this simulated case is of about 25 m s<sup>-1</sup> and the time constant of the cloud collection by snow calculated in section 2 is of the order of 5 min,

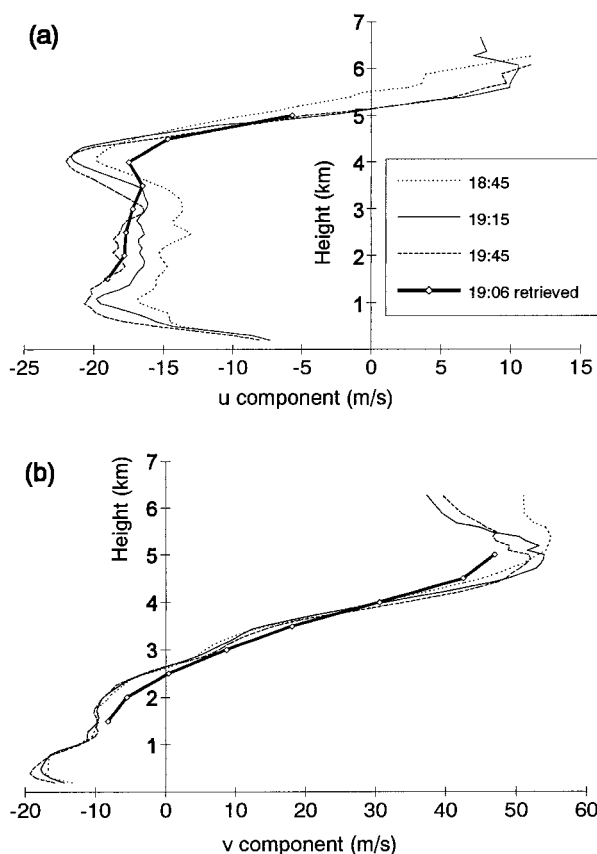


FIG. 6. Comparison of retrieved profiles of horizontal wind components at 1906 EST on 13 Mar 1993 with the 915-MHz wind profiler data: (a) *u* component, (b) *v* component.

the effect of the boundaries could be felt approximately 5–10 km inside the domain. Past this transitional region, the retrieved liquid water content inside the central domain should remain the same regardless of the value forced at the boundaries. It can be noted that numerical diffusion, introduced by cubic interpolation of the semi-Lagrangian advection scheme used in the model, also has some effect on the solution.

*d. Analysis of the results*

The two simulations are performed to demonstrate that the model-simulated field of snow precipitation reproduces correctly the radar observations with little sensitivity to the initial snow field within the domain once steady state is reached. Run 1 is performed with all the hydrometeor fields within the model domain starting at zero, whereas run 2 is initialized with the observed snow field. In run 1, within the first 10 min of simulation time, ice crystals are activated as the ascendant air generates supersaturation with respect to ice. Then, cloud water and snow appear. Cloud water peaks after 50 min, when snow starts to grow rapidly by the collection of SCW. The cloud water is depleted and an equilibrium

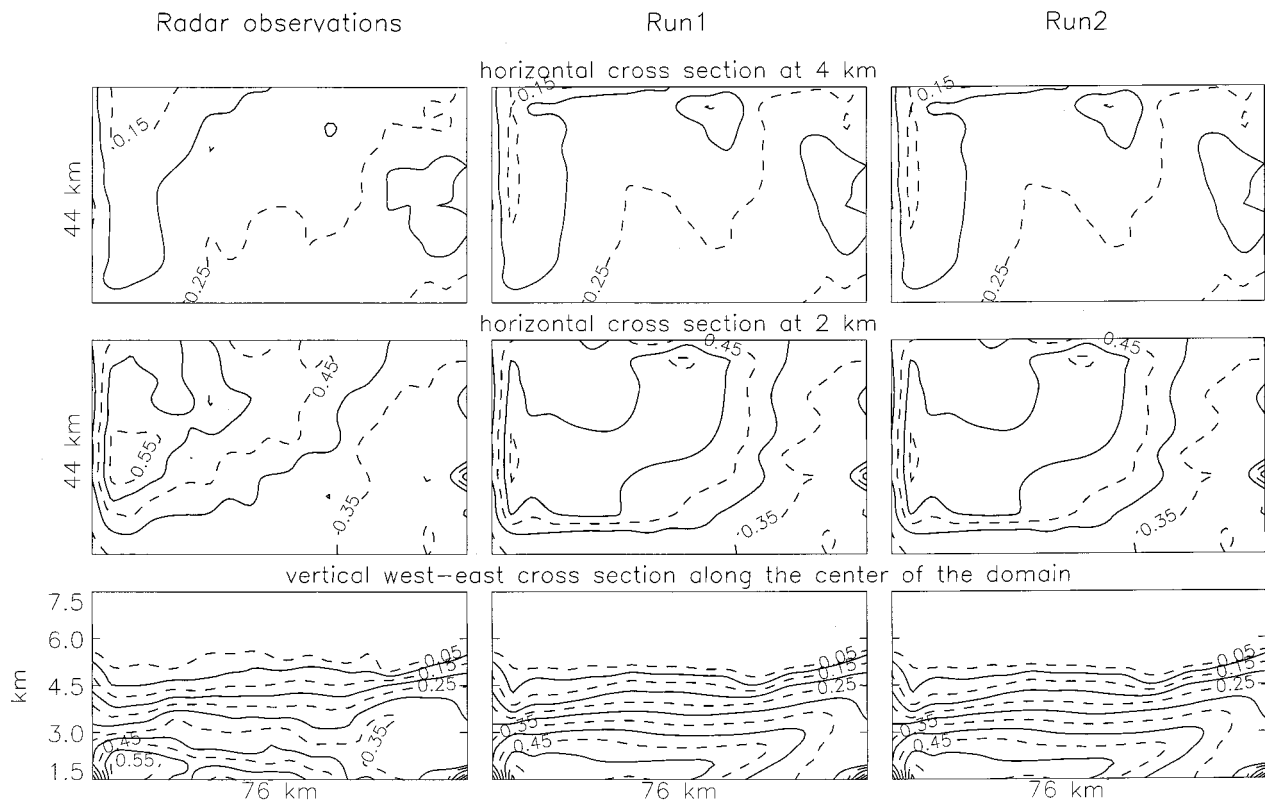


FIG. 7. Comparison between the observed snow field at 0006 UTC and the model outputs in run 1 and run 2 at two horizontal cross sections (at 4 and 2 km) and vertical west-east section taken along the center of the simulated domain. The contours representing the snow water content are plotted with  $0.05 \text{ g m}^{-3}$  intervals.

solution is obtained after nearly 2 h of simulation time (i.e., spinup time). In run 2, the initial snow field precipitates and is replaced by the snow generated by the model, resulting in the same equilibrium solution as obtained in run 1. Figure 7 shows the comparison of the observed snow field with the results of the two model runs after equilibrium is reached. There is almost no difference between the two runs. It is clear that the equilibrium state of the model is not sensitive to the initial distributions of the hydrometeors and the final pattern of the snow field is determined by the distribution of the wind field. At equilibrium, the model-simulated fields are practically independent of the parameterization scheme of the processes governing the very early stages of the evolution, that is, the ice initiation and snow autoconversion. However, this parameterization may influence the temporal evolution of the model outputs.

Furthermore, the model-predicted snow is very similar to the radar-observed snow field. This result gives strong credibility to the 3D winds derived by the retrieval method and strongly suggest that a kinematic model can be used to retrieve the content of the non-observed hydrometeors in a steady-state situation. The steady state is verified by good agreement of simulated and observed snow content field. This result provides

a self-consistency check for the diagnostic method. If the retrieval of vertical velocity is faulty, and if the radar snow content is not well estimated, the model-derived and radar-observed snow content cannot be similar.

No supercooled water is found in the simulations of this particular storm. This agrees with the results of 13 applied to any layer of the computational domain. The vertical air motions are not sufficiently intense to allow SCW production in the presence of the important observed snowfall [consistent with (3)].

## 7. Case study of 21 October 1993

### a. Presentation of the case and the wind retrieval results

During this day, several episodes of stratiform precipitation, associated with a warm front, moved over the Montreal area [see Turcotte (1994) for more details]. The simulated situation was sampled by the research aircraft from the University of Wyoming (King Air—B200) flying in the morning over Montreal. The aircraft was equipped with several scientific instruments, allowing various types of parameters to be measured including liquid water content with a CSIRO hot wire instrument. The presence of SCW was recorded by aircraft

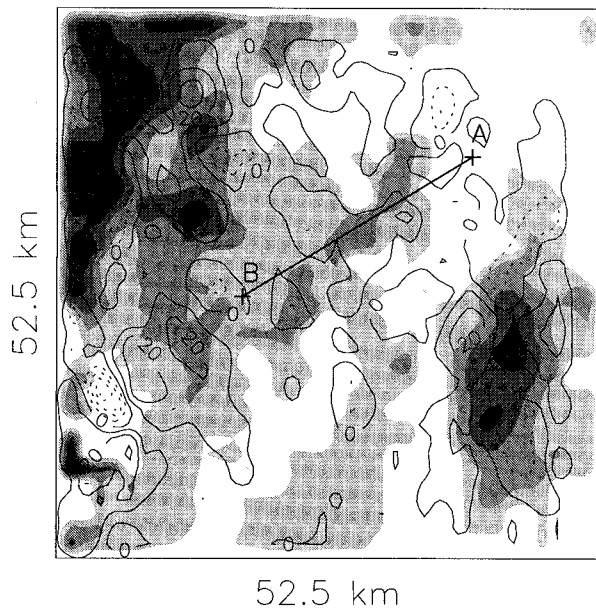


FIG. 8. The horizontal section at 4.5 km of the wind retrieval domain obtained for 1005 LST on 21 Oct 1993. The horizontal size of the domain is 52.5 km  $\times$  52.5 km, with the western boundary located at 20.5 km from the radar. The contours give the vertical air velocity contoured at 0.1 m s<sup>-1</sup> interval and shadings represent snow content corresponding to the observed reflectivity field, with values between 0.0 and 0.24 g m<sup>-3</sup> with 0.05 g m<sup>-3</sup> interval. The dark line represents the aircraft trajectory relative to the moving system.

between 0950 and 0955 EST at an average altitude of 4.61 km with ambient temperature around  $-5^{\circ}\text{C}$ . The icing that formed by accretion of supercooled droplets on the aircraft frame was not severe but was sufficient to observe the ice breaking off from the wings when the pilot activated the deicing mechanism installed on the leading edge of the wings. The obtained aircraft measurements are used to validate the SCW field generated by the model and, chiefly, that estimated by the proposed algorithm.

The 3D wind retrieval technique was applied to a domain of 52.5 km  $\times$  52.5 km around the aircraft trajectory, and located 20.5 km east of the radar, where Doppler radar data from MRO was available. Figure 8 presents the horizontal section of the wind retrieval domain at 4.5 km obtained for 1005 EST. The contours give the vertical motion and the shadings indicate the snow content calculated from the reflectivity field. The points A and B correspond to the extreme points of the aircraft track relative to the retrieval subdomain of the system. The retrieved horizontal wind field (not shown) is rather uniform and no wind shear is observed with height in this case. The system moves northeastward at a constant speed ( $u = 19 \text{ m s}^{-1}$  and  $v = 23 \text{ m s}^{-1}$ ).

*b. Numerical simulation*

The retrieved wind field initializes the 2-km-height domain of the model. To account for a strong horizontal

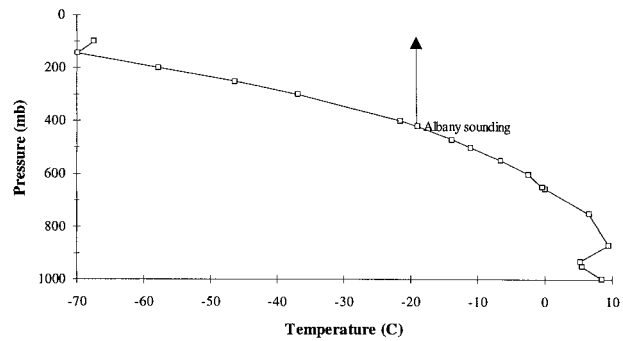


FIG. 9. Temperature profile for 1400 UTC 21 Oct 1993, as measured by the instrumented King Air in its ascent over Montreal. The profile is completed with the 1200 UTC Albany sounding above 420 mb. The melting layer is located at the 655-mb level, corresponding to a height at about 3.5 km.

advection the numerical domain follows the observed southwesterly movement of the system. The initial temperature field is given by the profile presented in Fig. 9, obtained up to 6 km from aircraft measurements and above from the 1200 UTC sounding of Albany. The water vapor mixing ratio in the domain is initialized by a profile of humidity at saturation with respect to ice. Initially, there is no condensate water within the domain. A zero value for the cloud liquid water mixing ratio is forced, throughout the numerical integration, on model boundaries.

The evolution of cloud liquid water and precipitating snow contents becomes steady state after about 1 h of simulation. The simulated cloud top is at  $-15^{\circ}\text{C}$  in this case. The comparison between the model-generated snow, after 1.5 h of simulation, and the snow derived from radar observations, is presented in the Fig. 10a. The fields shown are averaged over a 2.5-km distance along the aircraft trajectory, at a height of 4.625 km, the closest model level to the flight altitude. The good agreement between the simulated and observed data indicates that the model, at its equilibrium state, reproduces the snow amount along the aircraft trajectory. Thus, the self-consistency check is satisfactory. The difference at the first 5 km of the track is due to the absence of radar reflectivity observations in this region making the wind retrieval method not reliable.

The model-generated SCW content, averaged over 2.5 km, is shown in Fig. 10b. Since only snow and liquid water are produced by the model, the conditions under which the algorithm (13) is derived are fulfilled. In this case, the results can be compared with the in situ aircraft measurements.

*c. Diagnosed SCW content versus model-generated and observed values*

The retrieved  $w$  and  $M_s$ , together with the temperature ( $-5^{\circ}\text{C}$  as measured by aircraft) and pressure (56.8 kPa from the nearby sounding), are used in (13) in order to

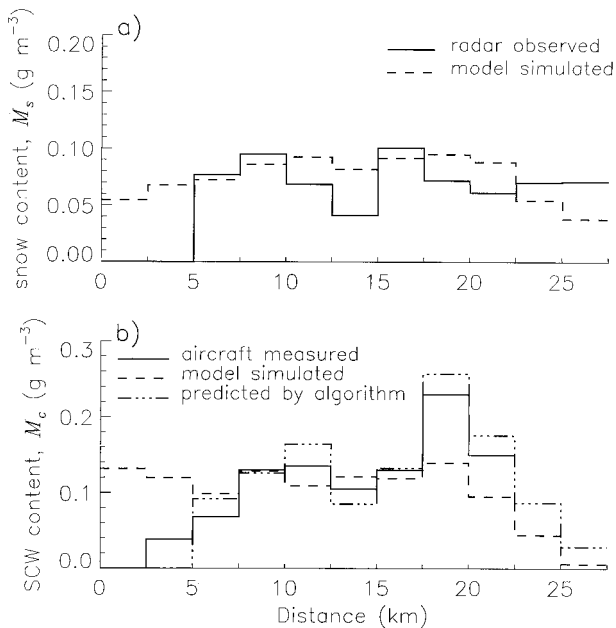


FIG. 10. Comparison between:(a) the observed and simulated snow content along the aircraft trajectory, and (b) the observed, simulated, and predicted-by-(13) SCW content.

find the field of  $M_c$  satisfying the balance conditions. The obtained values, averaged over 2.5 km along the aircraft track, are superposed in Fig. 10b on the values predicted by the model. The aircraft liquid water measurements averaged in the same scale are also shown. As mentioned earlier, the SCW amount is not calculated in the first 5 km of the track because of the absence of radar observations in this. During the last 5 km of track, the aircraft was descending, and thus the measurement of the SCW content corresponding to this period are not available.

As can be seen, the simulated amounts of SCW and the mean values of the predicted and the measured SCW contents are similar. However, even if the peak values of the two last fields are close, the simulated values are not so high. This may be partially explained by the fact that the three time-level semi-Lagrangian scheme used in the model is somewhat dissipative resulting in the degradation of finescale features. It can be also noted that both SCW diagnosed from (13) and model-generated content, whose averages are presented in Fig. 10b, are gridded fields (with the same 1.5-km horizontal resolution). Thus, their values represent an average over a grid while the aircraft was able to detect the variability on much smaller scale.

## 8. Conclusions

The timescale of the dynamics in stratiform precipitation systems is several hours, yet microphysical processes evolve much faster. The entire cycle of snow formation evolves in about 1 h. The time required for

cloud formation and to establish equilibrium conditions between the solid phase of precipitation and liquid cloud is of the order of 10 min. Therefore, once snow develops, microphysical processes are at a nearly steady state and close to equilibrium, within a system with slowly changing vertical motions. Thus, it is feasible to diagnose locally the presence and the amount of supercooled liquid water coexisting with snow if a good estimate of the vertical motion is available, and if the amount of snow is known with sufficient accuracy. Operational mesoscale numerical models with detailed microphysics parameterization could diagnose SCW content if their forecasting skills are adequate. Through radar data assimilation, we may obtain the level of skill necessary to reproduce a meteorological situation with sufficient temporal and spatial accuracy. Conversely, at the scales of a few kilometers, heuristic algorithms such as the one developed in this paper, based on real-time observations, may be more appropriate for nowcasting.

The purpose of this work was to demonstrate the feasibility of nowcasting of the SCW distribution using single-Doppler radar data. The computation of the SCW content at equilibrium with the observed snow is performed using a simplified local equilibrium condition. The vertical motion, required for the computations of the SCW content, is retrieved from single-Doppler observations. To verify that all assumptions are likely to be fulfilled in a given situation, sensitivity tests were performed using a kinematic numerical model driven by the retrieved winds. The model simulates the development of microphysical fields, including SCW and snow. Self-consistency is verified by comparing the model's output of snow content with the radar observations. The first simulation, reproducing a situation within the storm of 13–14 March 1993 showed that the model results were insensitive to initial conditions. A strong lateral advection of snow combined with a relatively slow adjustment of snow growth to the vertical motion causes the forcing of observed snow at the lateral boundaries necessary to retrieve the observed snow field within the domain. On the other hand, it was estimated that the liquid water content field in the interior of the domain is independent of the forcing at the boundaries. This is explained by the much shorter time constant associated with the processes involving SCW. The second simulated situation was encountered during the icing event recorded by aircraft. The retrieved liquid water content along the aircraft trajectory agrees well with the observations. However, even though the results of the comparison are very encouraging, verification against the observed SCW contents should be done in a wider range of situations.

The main limitation of the proposed technique is the requirement of radar-detectable snow. Also, the assumption of the negligible role of cloud ice crystals makes the method not valid in the regions above the levels where snow is generated and, in general, in a relatively colder atmosphere. The neglect of the possible

presence of ice crystals and graupel particles in the parcel will result in an overestimation of the retrieved SCW content since the deposition term will be larger after correcting for their presence. The collection of cloud water by precipitating graupel will also raise the riming rate.

Despite these limitations, the above retrieval algorithm may be useful for nowcasting of aircraft icing conditions. The method can be further improved with more detailed and complete microphysics on the one hand and more robust techniques for the estimation of vertical velocities and radar-derived snow contents on the other. Additional verifications with in situ measurements are needed.

Freezing precipitation is excluded from our analysis. Even if its presence constitutes a significant hazard to aviation, it is expected to occur much less frequently and under certain meteorological conditions (Politovich 1989; Stewart 1992; Pobanz et al. 1994). An algorithm that diagnoses icing conditions related to precipitable liquid water may be coupled with the algorithm developed in this work assuring better identification of aircraft icing conditions.

APPENDIX A

Microphysical Parameterization

The schematic representation of the microphysical processes active in our numerical experiments is shown in Fig. A1 (see appendix C for the description of the acronyms). The rate of each process describes here the rate of mass transfer between water categories per unit volume of air per unit of time ( $\text{kg m}^{-3} \text{s}^{-1}$ ). These rates are expressed in terms of moments of the distribution of particles forming a given water category. The  $x$ th moment of the  $k$  category particle distribution is defined by

$$F_k^{(x)} \equiv \int_{D_{\min}}^{D_{\max}} D_k^x N_k(D_k) dD_k \quad (\text{A1})$$

with  $D_k$  in m and  $N_k(D_k)$  in  $\text{m}^{-4}$ ,  $F_k^{(x)}$  is given here in

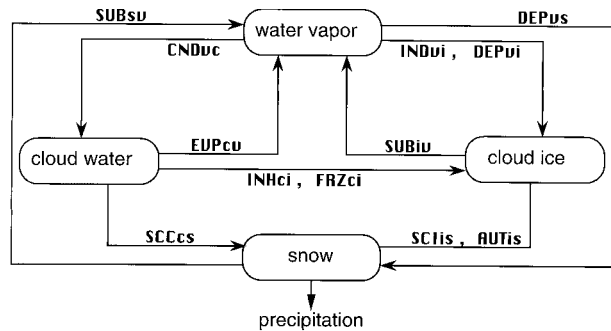


FIG. A1. Schematic representation of the microphysical processes active in the numerical simulations. Variables are defined in appendix C.

$\text{m}^{(\alpha-3)}$ . Assuming that smaller and larger sizes in the distribution are without importance, the lower and upper limits of integration in (A1) are replaced by 0 and  $\infty$ , respectively.

a. Hydrometeor characteristics

Cloud water and cloud ice are assumed to be monodisperse with a negligible terminal velocity. Ice particles are assumed to be spherical with a constant density of  $100 \text{ kg m}^{-3}$ . Precipitating snowflakes are supposed to be distributed according to an inverse exponential size distribution:

$$N_s(D_s) = N_{os} \exp[-\lambda D_s]. \quad (\text{A2})$$

Generally, the size distribution of snowflakes, excluding the smallest ones, fits this form well (e.g., Passarelli 1978). It is assumed that  $\lambda$  varies with snow content while  $N_{os}$  is independent of it. To take into account the broadening of the snow distribution due to the aggregation process at a higher temperature,  $N_{os}$  is considered temperature dependent as proposed by Cox (1988):

$$N_{os} = N_{oo} h(T)$$

with:

$$N_{oo} = 2 \times 10^6 \text{ m}^{-4} \quad \text{and}$$

$$h(T) = \exp\left(\frac{T_o - T}{8.18}\right), \quad (\text{A3})$$

where  $T_o = 273.15 \text{ K}$ . This parameterization is based on the observations of Houze et al. (1979). The relations between different moments of the exponential distribution and the snow mass content, calculated with (A3) at higher temperatures, are close to those found in ZOL.

The terminal fall speed of snow is expressed in the usual form:

$$V_s(D_s) = a D_s^b \left(\frac{\rho_o}{\rho}\right)^{1/2}, \quad (\text{A4})$$

where  $a = 5.1 \text{ m}^{(1-b)} \text{ s}^{-1}$  and  $b = 0.27$  from Locatelli and Hobbs (1974). The reference air density  $\rho_o = \rho(20^\circ\text{C}, 100 \text{ kPa}) = 1.2 \text{ kg m}^{-3}$ .

Here, we developed the expressions of two processes, which are used to derive the equation (13) that gives the estimation of the SCW amount. These processes describe the snow growth by collection of supercooled cloud water (SCCs), called riming, and by water vapor diffusion (DEPvs).

b. Snow riming (SCCs)

The formulation of the rate of mass transferred to snow by collected cloud liquid water is based on the geometric sweep-out concept under the assumption that the cloud droplets are very small compared to snowflakes and have negligible fall speed. The bulk rate of

the riming process, obtained for the entire distribution of snow, is given by

$$SCCcs = \frac{\pi}{4} \left( \frac{\rho_o}{\rho} \right)^{1/2} \bar{E}_{sc} a M_c F_s^{(2+b)}, \quad (A5)$$

where  $M_c$  is the liquid water content consisting of supercooled cloud droplets and is expressed in  $\text{kg m}^{-3}$ . The average value of the collection efficiency,  $\bar{E}_{sc}$ , is chosen to be 0.85.

*c. Water vapor diffusion on snow (DEPvs)*

The rate of mass transfer on snow particles by vapor diffusion is obtained assuming a thermal equilibrium on their surface: the rate of heat released by vapor deposition and freezing of the collected droplets is balanced by the rate of sensible heat conducted away from the particle surface. After integration over all range of size, the bulk rate of diffusional growth is obtained as

$$DEPvs = 2\pi\phi_i(S_i - 1)\{0.86F_s^{(1)} + 0.28\vartheta a^{1/2}F_s^{[(3+b)/2]}\} - \chi SCCcs. \quad (A6)$$

The expression for the snowflake ventilation coefficient used in the derivation of (A6) follows Hall and Pruppacher (1976). The three thermodynamic functions:  $\phi_i$ ,  $\vartheta$ , and  $\chi$  are defined as follows:

$$\phi_i(T, p) = \left[ \left( \frac{L_s}{R_v T} - 1 \right) \frac{L_s}{KT} + \frac{R_v T}{e_{si}(T)\psi} \right]^{-1}, \quad (A7)$$

$$\vartheta(T, p) = \rho_0^{1/4} (\rho \mu^2 \psi^4)^{-1/12}, \quad (A8)$$

$$\chi(T, p) = \frac{L_s L_f \phi_i}{R_v K T^2}, \quad (A9)$$

where the dynamic viscosity of air,  $\mu$ , from Rogers and Yau (1989) ( $\text{kg m}^{-1} \text{s}^{-1}$ ) is

$$\mu(T) = 1.72 \times 10^{-5} \frac{393.15}{T + 120} \left( \frac{T}{273.15} \right)^{1.5}, \quad (A10a)$$

the diffusivity of water vapor,  $\psi$ , from Hall and Pruppacher (1976) ( $\text{m}^2 \text{s}^{-2}$ ) is

$$\psi(T, p) = 2.11 \times 10^{-5} \frac{p_o}{p} \left( \frac{T}{273.15} \right)^{1.94}, \quad (A10b)$$

and the thermal conductivity of air,  $K$ , from Beard and Pruppacher (1971) ( $\text{J m}^{-1} \text{s}^{-1} \text{K}^{-1}$ ) is

$$K(T) = 4.19 \times 10^{-3} [5.69 + 0.017(T - 273.15)]. \quad (A10c)$$

In a supercooled environment, the saturation ratio,  $S_i$ , can be considered equal to the ratio of saturation vapor pressure over water and ice, given by the following approximate function of temperature (Rogers and Yau 1989):

$$S_i \approx \frac{e_s(T)}{e_{si}(T)} \approx \exp \left[ \frac{L_f}{273.15 R_v} \left( \frac{273.15}{T} - 1 \right) \right] \quad (\text{if } M_c > 0). \quad (A11)$$

The last term in (A6) represents a reduction of the depositional rate, in the presence of supercooled droplets. The release of heat during the freezing of collected droplets results in the increase of the particle surface temperature and, by this, the reduction of the vapor density excess. The function  $\chi(T, p)$  gives the ratio of the diffusional growth decrease that riming imposes to riming itself. The range of variability of  $\chi$  remains within 0.02–0.08, in the range of real atmospheric thermodynamic variables. It is almost linearly dependent on temperature but weakly dependent on pressure.

*d. Distribution moments expressed in terms of mass content*

The distribution moments, used in the expressions of process rates, depend on the type of assumed distribution function. For an inverse exponential size distribution of snow, given by (A2), the  $x$ th moment (in  $\text{m}^{x-3}$ ) can be expressed in terms of snow content (in  $\text{kg m}^{-3}$ ) as

$$F_s^{(x)} = a_x M_s^{b_x}, \quad (A12)$$

where  $b_x = (x + 1)/4$ ,  $a_x = \Gamma(x + 1)(\pi\rho_s)^{-b_x} N_{os}^{1-b_x}$ , and  $\Gamma$  is the complete gamma function. Here  $\rho_s$  and  $N_{os}$  have to be given in  $\text{kg cm}^{-3}$  and  $\text{m}^{-4}$ . With the aid of (A12), the relations describing the rates of water transfer via two snow growth processes, SCCcs and DEPvs, given by (A5) and (A6), respectively, can be expressed as a function of snow content,  $M_s$

$$SCCcs = \frac{\Gamma(3 + b)}{4\rho_s} (\pi\rho_s N_{os})^{(1-b)/4} a \bar{E}_{sc} \left( \frac{\rho_o}{\rho} \right)^{1/2} M_c M_s^{(3+b)/4} \quad (A13)$$

and

$$DEPvs = 2\pi\phi_i(S_i - 1) \times \left\{ 0.86 \left( \frac{N_{os}}{\pi\rho_s} \right)^{1/2} M_s^{1/2} + 0.28\Gamma \left( \frac{5+b}{2} \right) \left[ \frac{(N_{os})^{3-b}}{(\pi\rho_s)^{5+b}} \right]^{1/8} a^{1/2} \vartheta M_s^{(5+b)/8} \right\} - \chi SCCcs. \quad (A14)$$

From the last relation, it can be demonstrated that even if  $\chi$  is rather small, the term  $-\chi SCCcs$  can be relatively important to DEPvs and can introduce a nonnegligible correction to the expression of vapor deposition. At  $-5^\circ\text{C}$ , in a supercooled environment with a liquid water content of about  $0.5 \text{ g m}^{-3}$ , the diffusional mass transfer

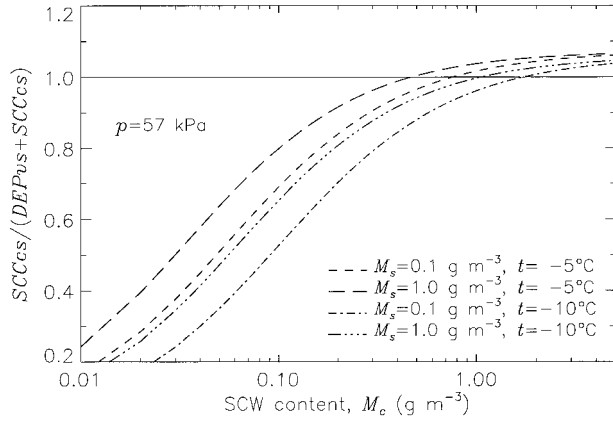


FIG. A2. Ratio of the growth rate of snow due to the riming to the total growth rate for two values of snow content. A pressure of 57 kPa and temperatures of  $-5^{\circ}$  and  $-10^{\circ}\text{C}$  are used in this calculation.

is reversed and becomes sublimation for practically any snow precipitation rate as can be seen in Fig. A2. Thus, a treatment of the diffusional growth of snowflakes that disregards the increase of their temperature caused by latent heat released during riming, may lead to completely incorrect values. Conversely, in computing total snow growth, comprising depositional and accretional components, the neglect of the term  $-\chi$  SCCcs can be absolutely justified since it represents less than 8% of the rate of growth by riming. In the areas where liquid water content is greater than about  $0.2 \text{ g m}^{-3}$ , the last mode of growth becomes the dominating source of the precipitation mass as shown in Fig. A2. Consequently, in calculations of the expected liquid water content from the relation (13), the approximation  $1 - \chi \approx 1$  is fully justified.

The results presented above indicate that within supercooled clouds at temperatures not very low (greater than about  $-10^{\circ}\text{C}$ ) and at SCW content higher than about  $0.5 \text{ g m}^{-3}$ , due to the high efficiency of liquid water collection by snow, the snow depositional growth becomes negligible and the removal of humidity by snow via vapor diffusion process becomes insignificant. Therefore, in these conditions the reduction of humidity below water saturation that results in liquid water evaporation and mass transfer from liquid to solid particles via water vapor, as suggested by the Bergeron process, does not occur if the solid particles are in the form of precipitation.

#### APPENDIX B

##### Uncertainties in Retrieved $M_c$

The proposed algorithm for inferring the SCW content requires assumed values of some microphysical parameters, such as  $N_{os}$  [or  $N_{oo}$  in (A3)],  $a$  and  $b$  in power-law fall speed relation (A4), and  $E_{sc}$  [introduced in (A5)]. Since the winter storm cloud conditions may vary in a wide range, one can speculate that the value of the

different microphysical quantities might differ from those assumed in our calculations. Here, we present the estimation of the uncertainties induced by the errors related to the fixed values of these parameters. To evaluate the sensitivity of the retrieved  $M_c$  to the intercept parameter  $N_{oo}$ , that represents  $N_{os}$  at  $0^{\circ}\text{C}$  as defined in (A3), we find from (13')

$$\frac{\partial M_c}{\partial N_{oo}} \approx -\frac{1-b}{4N_{oo}} \left[ \frac{1}{\beta M_s^{0.82}} (wG - \alpha C_1 M_s^{0.5}) + \frac{2}{1-b} \frac{1}{\beta M_s^{0.82}} \alpha C_1 M_s^{0.5} \right].$$

By incorporating (13') in the last equation, we obtain

$$\frac{\partial M_c}{\partial N_{oo}} \approx -\frac{1-b}{4N_{oo}} \left( M_c + \frac{2}{1-b} \frac{\alpha C_1}{\beta M_s^{0.32}} \right).$$

Introducing the approximate expression (5) for the snow deposition:  $\text{DEPvs} \approx \alpha C_1 M_s^{0.5}$ , and the expression of SCCcs, given by (5), leads to

$$\frac{\partial M_c}{M_c} \approx -\frac{1}{2N_{oo}} \left( \frac{1-b}{2} + \frac{\text{DEPvs}}{\text{SCCcs}} \right) \frac{\partial N_{oo}}{N_{oo}}.$$

From Fig. A2, it can be deduced that for  $M_c$  greater than about  $0.2 \text{ g m}^{-3}$  the ratio  $\text{DEPvs}/\text{SCCcs}$  can be neglected. Thus, we can write

$$\frac{\partial M_c}{M_c} \approx -\frac{1-b}{4N_{oo}} \frac{\partial N_{oo}}{N_{oo}} \approx 0.18 \frac{\partial N_{oo}}{N_{oo}} \quad \text{or}$$

$$\frac{M_c + \Delta M_c}{M_c} \approx \left( \frac{N_{oo} + \Delta N_{oo}}{N_{oo}} \right)^{0.18}. \quad (\text{B1})$$

Let  $M_c'(nN_{oo})$  denote the SCW content retrieved from (13) or (13') in the conditions of snowfall described by  $N_{os}$  for  $N'_{oo} = nN_{oo}$ , where  $N_{oo} = 2 \times 10^6 \text{ m}^{-4}$  as in the parameterization given in (A3). Then (B1) becomes

$$\frac{M_c'(nN_{oo})}{M_c(N_{oo})} \approx n^{0.18}.$$

It means that the change of  $N_{os}$  within one order of magnitude (or  $N_{oo}$  in our parameterization) leads to the error in  $M_c$  from (13) smaller than 50%. The ratio  $M_c'(nN_{oo})/M_c(N_{oo})$  calculated from (13) is plotted vs  $M_c(N_{oo})$  in Fig. B1. The relevant values of  $M_s$  and  $w$  are smaller than  $0.2 \text{ g m}^{-3}$  and  $1 \text{ m s}^{-1}$ , respectively. The curves show the results at two different temperatures:  $-5^{\circ}$  and  $-10^{\circ}\text{C}$  for two values of  $n$ : 0.5 and 5. This interval of  $n$  corresponds to the range of  $N_{os}$  most often reported in the literature.

For  $M_c$  smaller than about  $0.2 \text{ g m}^{-3}$ , associated with the situations when  $wG$  and  $\text{DEPvs}$  are very close, the error becomes greater. In these cases, the errors due to uncertainties in the estimates of  $M_s$  and  $w$  from radar observations are also large. However, we can deduce from (B1) that the predicted liquid water content is like-

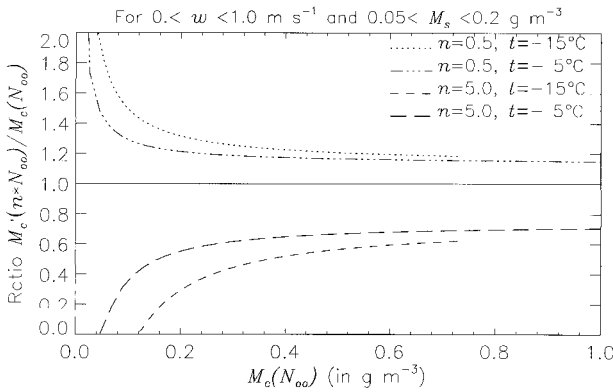


FIG. B1. Ratio  $M'_c(nN_{oo})/M_c(N_{oo})$  plotted against  $M_c(N_{oo})$  that denotes the value of  $M_c$  retrieved for the assumed  $N_{oo}$ . The curves show the results at two different temperatures:  $-5^\circ\text{C}$  and  $-10^\circ\text{C}$  for two values of  $n$ : 0.5 and 5. A pressure of 57 kPa is used in this calculation.

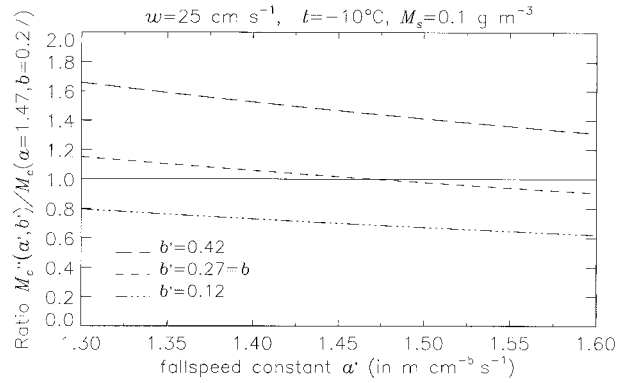


FIG. B2. Ratio  $M''_c(a', b')/M_c(a, b)$  plotted against the constant  $a'$  for three different values of  $b'$ : 0.27 (our original value), and 0.12 and 0.42.

ly to be overestimated through (13) if  $N_{os}$  is greater than the assumed value. The larger values of  $N_{os}$  correspond to higher concentrations containing smaller-sized particles. In these conditions, the snowfall rate deduced from a given radar reflectivity factor is overestimated. It leads to the underestimation of the amount of liquid water that coexists at equilibrium with the retrieved snow as calculated from (13). Thus, we have some compensation of the errors due to the intercept parameter value and to the  $Z-M_s$  relation uncertainties. Moreover, within the large radar sampled volume one is likely to find a broad range of  $N_{os}$ . Thus, as long as the value used is a good average value the errors should compensate.

To encompass most of possible values of  $E_{sc}$  describing the collection of cloud droplets by snow particles, we estimate  $E_{sc} = 0.85 \pm 0.15$ . Since the water content  $M_c$  calculated from (13) is inversely proportional to  $\beta$  (and  $\beta \propto E_{sc}$ ), we have  $|\Delta M_c/M_c| = |\Delta E_{sc}/E_{sc}|$  that gives the error of  $M_c$  within  $\pm 18\%$ . The  $\beta$  function is also proportional to  $a$ , that is, the fall speed constant. Some compensation of the uncertainties related to  $E_{sc}$  and  $a$  can be expected; laboratory investigations suggest that at the beginning of the riming,  $E_{sc}$  is a function of fall speed: the clogging of the snowflake's pores affects the airflow through the flake leading to a decrease of  $E_{sc}$ .

On the other hand, an increase in the exponent  $b$ , governing the particles fall speed variability, leads to a greater value of  $M_c$  than calculated. Let  $M_c(a, b)$  and  $M''_c(a', b')$  denote the SCW calculated from (13) with fall speed constants  $(a', b')$  and our original values  $(a, b)$ , respectively. In Fig. B2, the ratio  $M''_c(a', b')/M_c(a, b)$  is plotted versus the constant  $a'$  for three different values of  $b'$ : 0.27 (our original value), and 0.12 and 0.42. For snow, the great majority of the mass flux is contained within a narrow range of fall speed. Thus, it can be expected that the more important increase of  $a$  is associated with decrease of  $b$ . Therefore, we can conclude that the uncertainties related to the fall

speed constants may compensate each other to some degree.

APPENDIX C

List of Symbols

Symbol	Description	Value and units
AUTis	Autoconversion of cloud ice to snow	$\text{kg m}^{-3} \text{s}^{-1}$
$a$	Constant in formula (A4) for $V_s$ (Locatelli and Hobbs 1974)	$5.1 \text{ m}^{(b-1)} \text{ s}^{-1}$
$a_x$	Constant in relation (A12) for $F_s^{(x)}$	$\text{kg}^{-bx} \text{ m}^{x-3-3bx}$
$b$	Exponent in formula (A4) for $V_s$ (Locatelli and Hobbs 1974)	0.27
$b_x$	Exponent in relation (A12) for $F_s^{(x)}$	Dimensionless
CNDvc	Formation and condensational growth of liquid cloud water	$\text{kg m}^{-3} \text{s}^{-1}$
$C_1, C_2$	Functions of microphysical parameters in (5)	$\text{kg}^{-0.5} \text{ m}^{-0.5}, \text{kg}^{-0.66} \text{ m s}^{-0.5}$
$c_p$	Specific heat of air at constant pressure	$1004.6 \text{ J kg}^{-1} \text{ K}^{-1}$
DEPvi	Depositional growth of cloud ice	$\text{kg m}^{-3} \text{s}^{-1}$
DEPvs	Depositional growth of snow	$\text{kg m}^{-3} \text{s}^{-1}$
$D_k$	Equivalent diameter of $k$ category particle	m
$\bar{E}_{sc}$	Collection efficiency of snow particles for cloud droplets	0.85
$e_s$	Saturation vapor pressure over water	Pa
$e_{si}$	Saturation vapor pressure over ice	Pa
EVPcv	Evaporation of liquid cloud water	$\text{kg m}^{-3} \text{s}^{-1}$
$F_k^{(x)}$	$x$ th moment of the $k$ category particle distribution	$\text{m}^{x-3}$
FRZci	Freezing (heterogeneous) of cloud water to form cloud ice	$\text{kg m}^{-3} \text{s}^{-1}$

$G$	Negative of the product of air density with the vertical gradient of the saturation mixing ratio	$\text{kg m}^{-4}$	$\Gamma_w$	Moist-adiabatic lapse rate	$\text{K m}^{-1}$														
$g$	Gravitational acceleration	$9.81 \text{ m s}^{-2}$	$\varepsilon$	Ratio of molecular weight of water to molecular weight of air	0.622														
$h(T)$	Function [given by (A3)] describing $N_{os}$	Dimensionless	$\lambda$	Slope parameter of snow size distribution	$\text{m}^{-1}$														
INDvi	Ice nucleation by deposition	$\text{kg m}^{-3} \text{ s}^{-1}$	$\mu$	Dynamic viscosity of air	$\text{kg m}^{-1} \text{ s}^{-1}$														
INHci	Homogeneous ice nucleation by freezing of cloud water	$\text{kg m}^{-3} \text{ s}^{-1}$	$\rho$	Air density	$\text{kg m}^{-3}$														
$K$	Thermal conductivity of air	$\text{J m}^{-1} \text{ s}^{-1} \text{ K}^{-1}$	$\rho_0$	Reference air density	$1.2 \text{ kg m}^{-3}$														
$k$	Compressibility term, equal to $-\partial \ln \rho / \partial z$	$10^{-4} \text{ m}^{-1}$	$\rho_s$	Bulk density of snowflakes	$100 \text{ kg m}^{-3}$														
$L_f$	Latent heat of fusion	$3.34 \times 10^5 \text{ J kg}^{-1}$	$\rho_w$	Liquid water density	$1000 \text{ kg m}^{-3}$														
$L_s$	Latent heat of sublimation	$2.83 \times 10^6 \text{ J kg}^{-1}$	$\tau$	Time constant	s														
$L_v$	Latent heat of vaporization	$\text{J kg}^{-1}$	$\vartheta$	Thermodynamic function defined in (A8)	$\text{m}^{-1} \text{ s}^{0.5}$														
$M_c$	Mass content of cloud liquid water	$\text{kg m}^{-3}$	$\phi_i$	Thermodynamic function defined in (A7)	$\text{kg m}^{-1} \text{ s}^{-1}$														
$M_s$	Mass content of snow	$\text{kg m}^{-3}$	$\chi$	Thermodynamic function defined in (A9)	Dimensionless														
$N_k(D_k)$	Number concentration of $k$ category particles per unit diameter interval	$\text{m}^{-4}$	$\psi$	Water vapor diffusivity in air	$\text{m}^2 \text{ s}^{-1}$														
$N_{os}$	Intercept parameter of snow distribution	$\text{m}^{-4}$	APPENDIX D																
$N_{oo}$	Intercept parameter of snow distribution at $T_o$	$2 \times 10^6 \text{ m}^{-4}$	<b>Some Characteristics of the Used Doppler Radar</b>																
$p$	Air pressure	Pa	The data used in this work were collected at the J. S. Marshall Radar Observatory (MRO) Doppler radar located in the Montreal area. Technical specifications of the radar are provided in Table D1. Time series of reflectivity and radial velocity fields are obtained at 5-min intervals. The spatial resolution of the data is 1 km in range, $1^\circ$ in azimuth. Measurements are taken along 24 elevation angles.																
$r_s$	Saturation mixing ratio for water vapor with respect to water	$\text{kg kg}^{-1}$	TABLE D1. J. S. Marshall Observatory Doppler radar specifications.																
$R'$	Gas constant of dry air	$287.05 \text{ J kg}^{-1} \text{ K}^{-1}$	<table border="1" style="width: 100%; border-collapse: collapse;"> <tbody> <tr> <td>Wavelength:</td> <td>10.4 cm</td> </tr> <tr> <td>Peak power:</td> <td>800 kW</td> </tr> <tr> <td>Beamwidth:</td> <td><math>0.86^\circ</math></td> </tr> <tr> <td>Pulse repetition frequency (PRF) in Doppler mode:</td> <td>1 200 Hz</td> </tr> <tr> <td>Maximum unambiguous range:</td> <td>125 km</td> </tr> <tr> <td>Nyquist velocity:</td> <td><math>31.5 \text{ m s}^{-1}</math></td> </tr> <tr> <td>Time of volume scan:</td> <td>5 min.</td> </tr> </tbody> </table>			Wavelength:	10.4 cm	Peak power:	800 kW	Beamwidth:	$0.86^\circ$	Pulse repetition frequency (PRF) in Doppler mode:	1 200 Hz	Maximum unambiguous range:	125 km	Nyquist velocity:	$31.5 \text{ m s}^{-1}$	Time of volume scan:	5 min.
Wavelength:	10.4 cm																		
Peak power:	800 kW																		
Beamwidth:	$0.86^\circ$																		
Pulse repetition frequency (PRF) in Doppler mode:	1 200 Hz																		
Maximum unambiguous range:	125 km																		
Nyquist velocity:	$31.5 \text{ m s}^{-1}$																		
Time of volume scan:	5 min.																		
$R_v$	Gas constant of water vapor	$461.5 \text{ J kg}^{-1} \text{ K}^{-1}$																	
SCCs	riming of snow by cloud water	$\text{kg m}^{-3} \text{ s}^{-1}$																	
SCIis	Collection of cloud ice by snow	$\text{kg m}^{-3} \text{ s}^{-1}$																	
$S_i$	Saturation ratio relative to ice	Dimensionless																	
$S_s$	Microphysical snow source/sink	$\text{kg m}^{-3} \text{ s}^{-1}$																	
SUBiv	Sublimation of cloud ice	$\text{kg m}^{-3} \text{ s}^{-1}$																	
SUBsv	Sublimation of snow	$\text{kg m}^{-3} \text{ s}^{-1}$																	
$t$	Time	s																	
$T$	Air temperature	K ( $^\circ\text{C}$ )																	
$T_o$	Melting temperature	273.15 K																	
$V_s$	Terminal fall speed of snowflakes	$\text{m s}^{-1}$																	
$\bar{V}_s$	Distribution-averaged fall speed of snow	$\text{m s}^{-1}$																	
$w$	Vertical velocity	$\text{m s}^{-1}$																	
$w_{th}$	Vertical velocity threshold	$\text{m s}^{-1}$																	
$z$	Vertical coordinate	m																	
$Z$	Equivalent radar reflectivity factor	$\text{mm}^6 \text{ m}^{-3}$																	
$\alpha$	Thermodynamic function introduced in (5)	$\text{kg m}^{-1} \text{ s}^{-1}$	REFERENCES																
$\alpha_1, \alpha_2, \alpha_3$	Thermodynamic functions defined in (1)	$\text{m}^{-1}, \text{m}^3 \text{ kg}^{-1}, \text{m}^3 \text{ kg}^{-1}$	Beard, K. V., and H. R. Pruppacher, 1971: A wind tunnel investigation of the rate of evaporation of small water drops falling at terminal velocity in air. <i>J. Atmos. Sci.</i> , <b>28</b> , 1455–1466.																
$\beta$	Function of thermodynamical and microphysical parameters defined in (7)	$\text{kg}^{-0.82} \text{ m}^{2.46} \text{ s}^{-1}$	Burrows, D. A., 1992: Evaluation of a two-dimensional kinematic cloud model using data from a central Sierra Nevada orographic cloud system. <i>J. Appl. Meteor.</i> , <b>31</b> , 51–63.																
$\Gamma$	Complete gamma function	Dimensionless	Cooper, W. A., W. R. Sand, M. K. Politovich, and D. L. Veal, 1984: Effects of icing on performance of research aircraft. <i>J. Aircr.</i> , <b>21</b> , 708–715.																
$\Gamma_d$	Dry-adiabatic lapse rate	$0.982 \times 10^{-2} \text{ K m}^{-1}$	Cotton, W. R., G. J. Tripoli, R. M. Rauber, and E. A. Mulvihill, 1986: Numerical simulation of the effects of varying ice crystal nucleation rates and aggregation processes on orographic snowfall. <i>J. Climate Appl. Meteor.</i> , <b>25</b> , 1658–1680.																
			Cox, G. P., 1988: Modelling precipitation in frontal rainbands. <i>Quart. J. Roy. Meteor. Soc.</i> , <b>114</b> , 115–127.																

- Devulapalli, S. S. N., and J. L. Collett Jr., 1994: The influence of riming and frontal dynamics on winter precipitation chemistry in level terrain. *Atmos. Res.*, **32**, 203–213.
- Dixon, R. W., L. Mosimann, B. Oberholzer, J. Staehelin, A. Waldvogel, and J. L. Collett Jr., 1995: The effect of riming on the ion concentration of winter precipitation. 1. A quantitative analysis of field measurements. *J. Geophys. Res.*, **100**, 11 517–11 527.
- Ferrier, B. S., 1994: A double-moment multiple-phase four-class bulk ice scheme. Part I: Description. *J. Atmos. Sci.*, **51**, 249–280.
- Gayet, J.-F., P. Personne, and D. Guffond, 1992: Le givrage atmosphérique. *Météorologie*, **43–44**, 18–23.
- Hall, W. D., and H. R. Pruppacher, 1976: The survival of ice particles falling from cirrus clouds in subsaturated air. *J. Atmos. Sci.*, **33**, 1995–2006.
- Hallett, J., and S. C. Mossop, 1974: Production of secondary ice particles during the riming process. *Nature*, **249**, 26–28.
- Heggli, M. F., L. Vardiman, R. E. Stewart, and A. Huggins, 1983: Supercooled liquid water and ice crystal distributions within Sierra Nevada winter storms. *J. Climate Appl. Meteor.*, **22**, 1875–1886.
- Heysmsfield, A. J., 1977: Precipitation development in stratiform ice clouds: A microphysical and dynamical study. *J. Atmos. Sci.*, **34**, 367–381.
- Houze, R. A., Jr., P. V. Hobbs, P. H. Herzegh, and D. B. Parsons, 1979: Size distributions of precipitation particles in frontal clouds. *J. Atmos. Sci.*, **36**, 156–162.
- Huo, Z., D.-L. Zhang, J. Gyakum, and A. Staniforth, 1995: A diagnostic analysis of the superstorm of March 1993. *Mon. Wea. Rev.*, **123**, 1740–1761.
- Kessler, E., 1969: *On the Distribution and Continuity of Water Substance in Atmospheric Circulations*, Meteor. Monogr., No. 32, Amer. Meteor. Soc., 84 pp.
- Kilambi, E., S. Laroche, and I. Zawadzki, 1995: An operational 3D wind retrieval algorithm. Preprints, *27th Conf. on Radar Meteorology*, Vail, CO, Amer. Meteor. Soc., 258–260.
- Laroche, S., and I. Zawadzki, 1994: A variational analysis method for the retrieval of three-dimensional wind field from single-Doppler radar data. *J. Atmos. Sci.*, **51**, 2664–2682.
- Locatelli, J. D., and P. V. Hobbs, 1974: Fallspeeds and masses of solid precipitation particles. *J. Geophys. Res.*, **79**, 2185–2197.
- Meyers, M. P., P. J. DeMott, and W. R. Cotton, 1992: New primary ice-nucleation parameterizations in an explicit cloud model. *J. Appl. Meteor.*, **31**, 708–721.
- Modica, G. D., S. T. Heckman, and R. M. Rasmussen, 1994: An application of an explicit microphysics mesoscale model to a regional icing events. *J. Appl. Meteor.*, **33**, 53–63.
- Murakami, M., 1990: Numerical modeling of dynamical and microphysical evolution of an isolated convective cloud. *J. Meteor. Soc. Japan*, **68**, 107–128.
- , Y. Yamada, T. Matsuo, H. Mizuno, and K. Morikawa, 1992: Microphysical structures of warm-frontal clouds—The 20 June 1987 case study. *J. Meteor. Soc. Japan*, **70**, 877–894.
- Passarelli, R. E., Jr., 1978: Theoretical and observational study of snow-size spectra and snowflake aggregation efficiencies. *J. Atmos. Sci.*, **35**, 882–889.
- Perkins, P. J., 1995: Developments in aircraft ice protection during sixty years of research. *Int. Icing Symp.*, Montreal, PQ, Canada, Amer. Helicopter Soc., 5-1–5-8.
- Pobanz, B. M., J. D. Marwitz, and M. K. Politovich, 1994: Conditions associated with large-drop regions. *J. Appl. Meteor.*, **33**, 1366–1372.
- Politovich, M. K., 1989: Aircraft icing caused by large supercooled droplets. *J. Appl. Meteor.*, **28**, 856–868.
- Pruppacher, H. R., and J. D. Klett, 1997: *Microphysics of Clouds and Precipitation*. Kluwer Academic, 955 pp.
- Rasmussen, R., and Coauthors, 1992: Winter Icing and Storm Project (WISP). *Bull. Amer. Meteor. Soc.*, **73**, 951–974.
- Rauber, R. M., and A. Tokay, 1991: An explanation for the existence of supercooled water at the top of cold clouds. *J. Atmos. Sci.*, **48**, 1005–1023.
- , D. Feng, L. O. Grant, and J. B. Snider, 1986: The characteristics and distribution of cloud water over the mountains of northern Colorado during wintertime storms. Part I: Temporal variations. *J. Climate Appl. Meteor.*, **25**, 468–488.
- Rogers, R. R., and M. K. Yau, 1989: *A Short Course in Cloud Physics*. Pergamon Press, 293 pp.
- , S. A. Cohn, W. L. Ecklund, J. S. Wilson, and D. A. Carter, 1994: Experience from one year of operating a boundary-layer profiler in the center of a large city. *Ann. Geophys.*, **12**, 529–540.
- Sassen, K., K. N. Liou, S. Kinne, and M. Griffin, 1985: Highly supercooled cirrus cloud water: Confirmation and climatic implications. *Science*, **227**, 411–413.
- , A. W. Huggins, A. B. Long, J. B. Snider, and R. Meitin, 1990: Investigations of a winter mountain storm in Utah. Part II: Mesoscale structure, supercooled liquid water development, and precipitation processes. *J. Atmos. Sci.*, **47**, 1323–1350.
- Stewart, R. E., 1992: Precipitation types in the transition region of winter storms. *Bull. Amer. Meteor. Soc.*, **73**, 287–296.
- Tremblay, A., A. Glazer, W. Szyrmer, G. Isaac, and I. Zawadzki, 1995: Forecasting of supercooled clouds. *Mon. Wea. Rev.*, **123**, 2098–2113.
- Turcotte, F. A., 1994: A method for aircraft icing diagnosis in precipitation. M.S. thesis, McGill University, 62 pp.
- Wahba, G., and J. Wendelberger, 1980: Some new mathematical methods for variational objective analysis using splines and cross validation. *Mon. Wea. Rev.*, **108**, 1122–1143.
- Waldvogel, A., W. Henrich, and L. Mosimann, 1993: New insight into the coupling between snow spectra and raindrop size distributions. Preprints, *26th Int. Conf. on Radar Meteorology*, Norman, OK, Amer. Meteor. Soc., 602–604.
- Zawadzki, I., L. Ostiguy, and R. Laprise, 1993a: Retrieval of the microphysical properties in a CASP storm by integration of a numerical kinematic model. *Atmos.–Ocean*, **31**, 201–233.
- , P. Zwack, and A. Frigon, 1993b: A study of a CASP storm: Analysis of radar data. *Atmos.–Ocean*, **31**, 175–199.